





A second Wpl1 anti-cohesion pathway requires dephosphorylation of fission yeast kleisin Rad21 by PP4

Adrien Birot^{1,†}, Karen Eguinta^{1,†} , Stéphanie Vazquez¹, Stéphane Claverol², Marc Bonneu², Karl Ekwall³, Jean-Paul Javerzat^{1,*}  & Sabine Vaur¹

Abstract

Cohesin mediates sister chromatid cohesion which is essential for chromosome segregation and repair. Sister chromatid cohesion requires an acetyl-transferase (Eso1 in fission yeast) counteracting Wpl1, promoting cohesin release from DNA. We report here that Wpl1 anti-cohesion function includes an additional mechanism. A genetic screen uncovered that Protein Phosphatase 4 (PP4) mutants allowed cell survival in the complete absence of Eso1. PP4 co-immunoprecipitated Wpl1 and cohesin and Wpl1 triggered Rad21 de-phosphorylation in a PP4-dependent manner. Relevant residues were identified and mapped within the central domain of Rad21. Phospho-mimicking alleles dampened Wpl1 anti-cohesion activity, while alanine mutants were neutral indicating that Rad21 phosphorylation would shelter cohesin from Wpl1 unless erased by PP4. Experiments in post-replicative cells lacking Eso1 revealed two cohesin populations. Type 1 was released from DNA by Wpl1 in a PP4-independent manner. Type 2 cohesin, however, remained DNA-bound and lost its cohesiveness in a manner depending on Wpl1- and PP4-mediated Rad21 de-phosphorylation. These results reveal that Wpl1 antagonizes sister chromatid cohesion by a novel pathway regulated by the phosphorylation status of the cohesin kleisin subunit.

Keywords cohesin; fission yeast; Protein Phosphatase 4; WAPL

Subject Categories Cell Cycle; Post-translational Modifications, Proteolysis & Proteomics

DOI 10.15252/embj.201696050 | Received 9 November 2016 | Revised 10 March 2017 | Accepted 27 March 2017 | Published online 24 April 2017

The EMBO Journal (2017) 36: 1364–1378

Introduction

To ensure proper chromosome segregation in mitosis and meiosis, sister chromatids are held together from S phase and until nuclear

division by cohesin, a ring-shaped protein complex also required for chromosome organization, gene expression and DNA repair (Nasmyth & Haering, 2009; Peters & Nishiyama, 2012; Remeseiro & Losada, 2013). Defects in cohesin functions in human can lead to severe pathologies such as Down syndrome, developmental defects and cancer (Watrin *et al*, 2016). The ring shape of cohesin is formed by two coiled-coil SMC proteins (Structural Maintenance of Chromosomes, Psm1 and Psm3 in fission yeast) that dimerize through their hinge domain at one end. At the other end, the SMCs fold into head domains which bind together in an ATP-dependent manner. A third protein, the kleisin Rad21/Scc1/Mcd1, bridges the two SMCs heads. Pds5, Wpl1 and Psc3 are conserved additional subunits that bind to Rad21 (Nasmyth & Haering, 2009; Peters & Nishiyama, 2012; Remeseiro & Losada, 2013).

How cohesin ensures sister chromatid cohesion is still controversial. Cohesin is able to concatenate sister DNA molecules (Haering *et al*, 2008) leading to a model in which a single cohesin ring encircles sister chromatids. Alternative models propose that cohesin may function as dimers, each ring encircling a single chromatid or even as interacting oligomers (Huang *et al*, 2005; Surcel *et al*, 2008; Zhang *et al*, 2008; Eng *et al*, 2015). Although it is clear that cohesin function involves DNA capture, the conformation of cohesive cohesin remains elusive and may not be unique. DNA capture by cohesin requires ATP hydrolysis by the SMCs and a loading complex called Mis4/Ssl3 in fission yeast. Conversely, DNA escape from cohesin is thought to involve DNA passage through two interfaces. ATP hydrolysis by the SMCs would disengage the SMC's heads, while Wpl1 would disrupt the Psm3-Rad21 interface in a reaction involving Pds5, Psc3 and Psm3 head domain (Chan *et al*, 2012; Peters & Nishiyama, 2012; Gligoris *et al*, 2014; Huis in 't Veld *et al*, 2014; Murayama & Uhlmann, 2015; Beckouet *et al*, 2016).

Sister chromatid cohesion is essential for chromosome segregation implying that cohesion must be stable enough to last from S phase and until nuclear division, a time frame ranging from hours in vegetative cells to decades in human oocytes. Concomitantly with the establishment of sister chromatid cohesion in S phase, a

¹ Institut de Biochimie et Génétique Cellulaires, UMR 5095 CNRS – Université de Bordeaux, Bordeaux, France

² Centre Génomique Fonctionnelle de Bordeaux, Université de Bordeaux, Bordeaux, France

³ Department of Biosciences and Nutrition, Karolinska Institutet, Huddinge, Sweden

*Corresponding author. Tel: +33 5 56999026; E-mail: JP.Javerzat@ibgc.cnrs.fr

[†]These authors contributed equally to this work

sub-population of cohesin becomes stably bound to DNA and mediates sister chromatid cohesion (Gerlich *et al*, 2006; Bernard *et al*, 2008; Feytout *et al*, 2011; Chan *et al*, 2012; Vaur *et al*, 2012). This requires a conserved acetyl-transferase (Eso1 in fission yeast) that acetylates two conserved lysine residues within SMC3 globular head domain (Peters & Nishiyama, 2012). Recent evidence indicates that SMC3 acetylation would prevent DNA release from cohesin by preventing ATP hydrolysis by the SMCs (Murayama & Uhlmann, 2015; Beckouet *et al*, 2016; Elbatsh *et al*, 2016).

In mammals, the cohesin acetyl-transferases down-regulate Wpl1 anti-cohesion function by promoting Sororin-mediated eviction of Wpl1 from cohesin (Nishiyama *et al*, 2010). Sororin is not conserved through evolution and is apparently lacking in fungi, raising the possibility that Wpl1 anti-cohesion function might be regulated by an ancient, yet to be discovered, ubiquitous pathway.

In fission yeast, the *eso1* gene is essential for sister chromatid cohesion and cell viability but dispensable when the *wpl1* gene is deleted (Tanaka *et al*, 2000; Feytout *et al*, 2011). Likewise, the acetyl-mimicking allele *psm3*^{K105NK106N} allows cell survival in the absence of Eso1. However, the thermosensitive *eso1-H17* mutant is deficient for Psm3^{K106} acetylation even at the permissive temperature and the *psm3*^{K105RK106R} non-acetylatable mutant is viable, indicating that Eso1 might counteract Wpl1 through another mechanism besides Psm3 acetylation (Feytout *et al*, 2011; Kagami *et al*, 2011).

To search for novel components of the pathway, we made a genetic screen for mutants able to bypass Eso1 function and uncovered *pph3*, encoding the catalytic subunit of PP4. PP4 is a member of the PP2A family of Ser/Thr phosphoprotein phosphatases conserved from yeast to human. The common form of PP4 comprises a catalytic and two regulatory subunits and is involved in a variety of cellular processes, including chromosome biology and cell cycle progression (Cohen *et al*, 2005). In *Schizosaccharomyces pombe*, there is only one known regulatory subunit called Psy2, annotated as the homologue of *Saccharomyces cerevisiae* Psy2 and the human PP4 regulatory subunits 3A and 3B.

Here, we present evidence that PP4 is integral to Wpl1 function and identified Rad21 as a relevant PP4 substrate. We identified key residues within Rad21 that must be de-phosphorylated to authorize Wpl1-dependent loss of sister chromatid cohesion. Surprisingly, PP4 is not required for Wpl1-mediated cohesin release from DNA. Rather, our data reveal the existence of a sub-population of cohesin whose cohesiveness is abolished by the combined action of Wpl1- and PP4-mediated de-phosphorylation of Rad21 without apparent cohesin removal from DNA.

Results

PP4 ablation bypasses the requirement for the otherwise essential Eso1 acetyl-transferase

Through a genetic screen for suppressors of the thermosensitive phenotype of *eso1-H17*, we recovered mutations in *psm3*, *wpl1*, *pds5* and *pdc3* that is in all known components of the Wpl1-Eso1 pathway (Fig 1). A mutation within a fifth gene, *p-ph3*, encoding the catalytic subunit of PP4 was also recovered. Deletion of the genes encoding *p-ph3* or its regulatory subunit *psy2* suppressed the thermosensitive growth defect of *eso1-H17* (Fig 1D) and remarkably,

allowed cell survival in the complete absence of the otherwise essential *eso1* gene (Fig 1E). The cell growth assays indicated that Eso1 bypass by PP4 mutants was incomplete, but the additional deletion of *wpl1* restored wild-type growth (Fig 1F), indicating that Wpl1 retained some function in the absence of PP4. Conversely, this suggested that Wpl1 might not be fully functional when PP4 is ablated, thereby allowing cell survival in the absence of Eso1.

PP4 is required for Wpl1 anti-cohesion function

To test this idea, we set up an *in vivo* assay for Wpl1 anti-cohesion activity. In budding yeast, Wpl1 induction after S phase in an *eco1-1* mutant destroyed sister chromatid cohesion (Chan *et al*, 2012). We constructed a strain in which Wpl1 expression is induced by tetracycline (*tet07-wpl1-MYC*). As expected, Wpl1 induction in G2 cells did not affect chromosome segregation during the ensuing mitosis when the experiment was made in an *eso1*⁺ background (Fig 2A). By contrast in an *eso1Δ* strain, ~90% of mitotic cells showed a severe chromosome segregation defect. Importantly, this phenotype was attenuated when *psy2* was deleted (33% aberrant mitoses, Fig 2A). A similar level of suppression was observed in a *p-ph3Δ* background and no additive effect was seen when both *p-ph3* and *psy2* were deleted (Fig EV1), consistent with the notion that each individual deletion mutant abrogates PP4 function. To directly assess the status of sister chromatid cohesion, cells were arrested at metaphase and cohesion monitored by FISH using a probe proximal to the centromere of chromosome 2 (cen2FISH). Wpl1 induction provoked a pronounced cohesion defect, which was significantly attenuated by *p-ph3* deletion (Fig 2B), arguing that PP4 is required for Wpl1 anti-cohesion function.

Wpl1 triggers Rad21 de-phosphorylation in a PP4-dependent manner

Co-immunoprecipitation experiments from total protein extracts showed that Psy2-FLAG pulled down Wpl1 and all three core cohesin components suggesting that cohesin and/or associated factors might be PP4 substrates (Fig 3A and B). Consistently, Rad21 electrophoretic mobility was modified in PP4 mutants. In wild-type cycling cells [which are mainly in the G2 phase of the cell cycle (Carlson *et al*, 1999)], Rad21 is present as several phospho-isoforms (Fig 3C; Birkenbihl & Subramani, 1995; Adachi *et al*, 2008). By contrast, the slowest-migrating Rad21 species accumulated in *p-ph3Δ* cells (Fig 3C). The mobility shift was due to phosphorylation since it was abrogated by phosphatase treatment (Fig 3D). Importantly, Rad21 showed a similar pattern in *wpl1Δ* and *pds5Δ* cells (Fig 3C), suggesting that Rad21 de-phosphorylation is integral to Wpl1 function. Consistently, the Wpl1 induction experiments showed that the bulk of Rad21 is de-phosphorylated in a Wpl1- and PP4-dependent manner (Fig 3E). Wpl1 activity is therefore coupled with PP4-dependent Rad21 de-phosphorylation. It is worth mentioning that the pattern of Rad21 phosphorylation was not altered in *psm3* acetylation mutants (Fig 3C), suggesting that this function of Wpl1 is not controlled by Psm3 acetylation.

Identification of key phosphorylated residues within Rad21

To identify the relevant residues, Rad21 was purified from wild-type and *p-ph3Δ* cells and analysed by mass spectrometry. A total

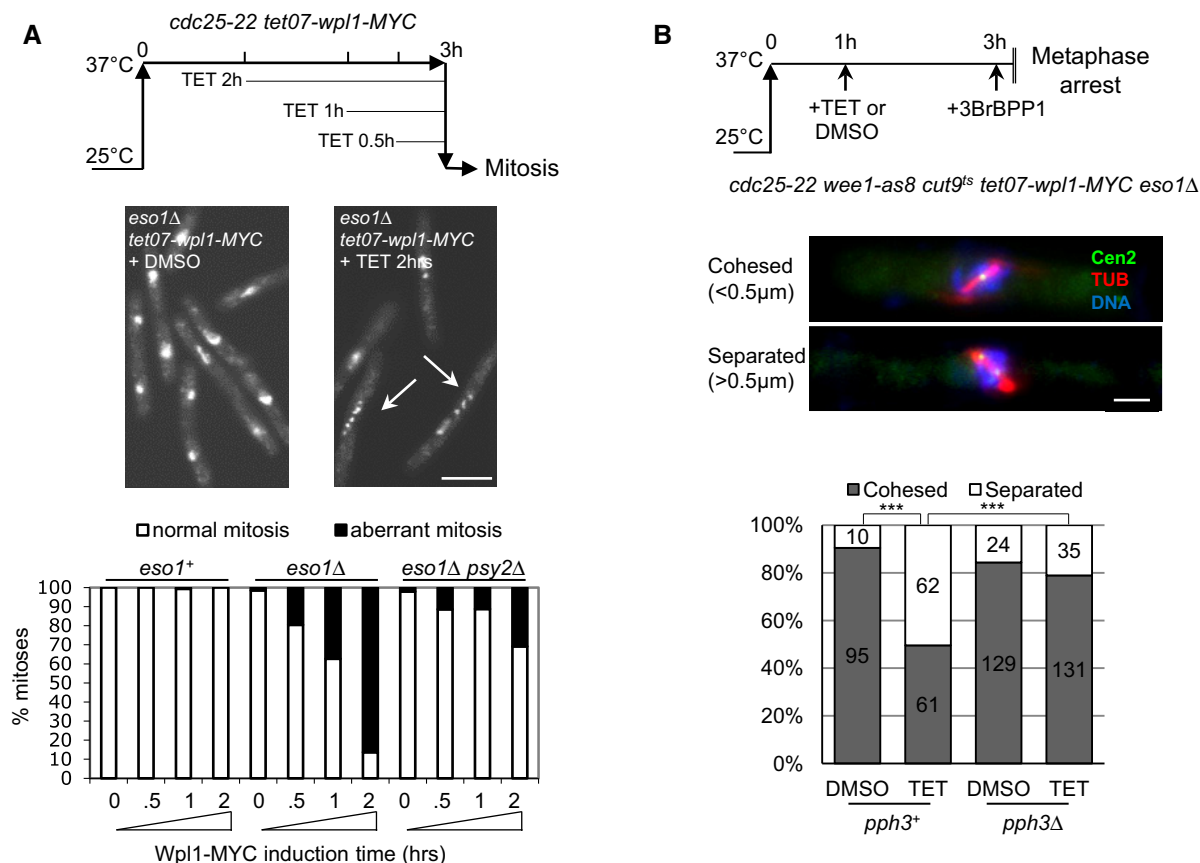


Figure 2. Wpl1 anti-cohesion function requires PP4.

A Wpl1 induction in *eso1Δ* G2 cells induces loss of sister chromatid cohesion and aberrant mitosis in a PP4-dependent manner. Cycling *cdc25-22* cells (~80% G2 cells) were shifted to 37°C to prevent mitotic entry, and Wpl1-MYC was induced at the indicated time-points. Cells were released into mitosis by shifting the temperature back to 25°C, DNA was stained with DAPI, and aberrant mitoses (arrows) were scored. Scale bar 10 μm.

B Wpl1-MYC was induced for 2 h after which time Wee1-as8 was inhibited with 3BrBPP1 to override the *cdc25-22* arrest. Cells progressed into M phase at 37°C and were arrested at metaphase by the thermosensitive APC mutation *cut9^{ts}*. Cells were fixed, tubulin stained to visualize the mitotic spindle and sister chromatid cohesion was monitored by FISH using a probe proximal to the centromere of chromosome 2. Scale bar 2 μm. ****P* < 0.0001 two-sided Fisher's exact test with α < 0.05. The number of metaphase cells examined is indicated within the graph.

mutant sequences were inserted at the endogenous *rad21* locus to create *rad21* phospho-mutants. Seven *rad21* alleles were found to suppress the thermosensitive phenotype of *eso1-H17* (Fig 4C and D). Sequence analysis revealed that all encoded a glutamic acid at position 163 with several suppressors having an additional phospho-mimicking residue at positions 164 or/and 165 (Fig 4C). To confirm this assumption, new *rad21* alleles were generated. A single S to E change at position 163 was sufficient to reduce the thermosensitive phenotype of *eso1-H17*. A better suppression was observed with an additional phospho-mimicking residue at position 164 or 165, and no further suppression was observed with the triple substituted allele *rad21-163E164E165E* (Fig 4E). We therefore focused on the *rad21-S163S164* substitution mutants.

It should be noted at this stage that *pph3Δ* is a better *eso1-H17* suppressor than *rad21-163E164E* and *pph3Δ* is epistatic on *rad21-163E164E* (Fig 5A), indicating that PP4 must have other relevant substrates. The alanine substituted allele *rad21-163A164A* exacerbated the thermosensitive phenotype of *eso1-H17* and partially compromised the suppression by *pph3Δ*, arguing that persistent

phosphorylation of Rad21-S163S164 is part of the mechanism by which *pph3Δ* suppresses *eso1-H17*. Finally, *wpl1Δ* was epistatic on *rad21-163A164A* and *rad21-163E164E* for *eso1-H17* suppression (Fig 5B), consistent with the notion that the phosphorylation status of Rad21 modulates Wpl1 function.

To assess the effect of Rad21 phosphorylation on Wpl1 activity, we used the *in vivo* Wpl1 anti-cohesion assay. As before, Wpl1 was induced in *eso1Δ* G2 cells and sister chromatid cohesion was assayed by cen2FISH at metaphase (Fig 5C). Wpl1 anti-cohesion activity was reduced in *rad21-163E164E*, largely mimicking the effect of *pph3Δ*, while *rad21-163A164A* was essentially neutral. This indicates that Rad21 phosphorylation *per se* is dispensable for sister chromatid cohesion but protects sister chromatid cohesion from Wpl1 when de-phosphorylation is prevented. Importantly *pph3Δ* suppression was compromised in a *rad21-163A164A* background (Fig 5C), consistent with PP4 acting through the de-phosphorylation of these two residues. Collectively, these data argue that Wpl1 is coupled with PP4-dependent de-phosphorylation of serine residues within the PISSS motif of Rad21 and this event is required for Wpl1 anti-cohesion function.

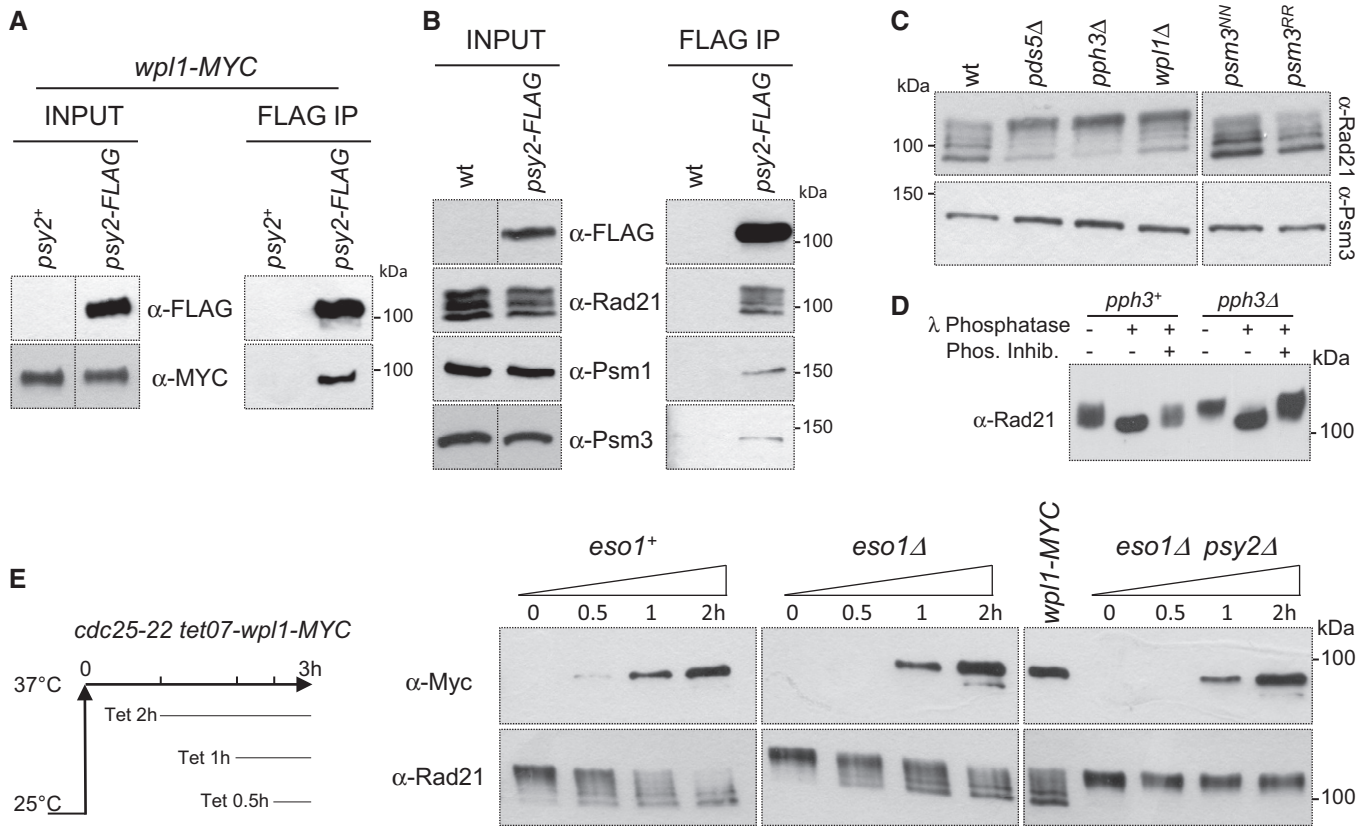


Figure 3. Wpl1 activity is coupled with PP4-dependent de-phosphorylation of Rad21.

A The regulatory PP4 subunit Psyl2 co-immunoprecipitates Wpl1 from total protein extracts.
 B Psyl2-FLAG co-immunoprecipitates all three core cohesin subunits from total protein extracts.
 C Rad21 is hyper-phosphorylated in *pph3*, *pds5* and *wpl1* deletion mutants but not in *psm3* acetyl-mutants.
 D *In vitro* treatment with λ phosphatase of Rad21-9PK immunoprecipitated from the indicated strains shows that Rad21 mobility shift is due to phosphorylation.
 E Western blot analysis of total protein extracts showing that *tet07-wpl1-MYC* induction in G2 cells triggers PP4-dependent Rad21 de-phosphorylation. A *cdc25-22 wpl1-MYC* control strain was included (right panel) showing that the amount of Wpl1-MYC produced from *tet07-wpl1-MYC* after 2 h is similar to that produced from *wpl1-MYC*.

Source data are available online for this figure.

Wpl1 induction experiments in *eso1*-deleted cells uncover two cohesin populations

Wpl1 is known to promote cohesin release from DNA, a straightforward mechanism for disrupting sister chromatid cohesion (Gandhi *et al*, 2006; Kueng *et al*, 2006; Bernard *et al*, 2008; Chan *et al*, 2012; Murayama & Uhlmann, 2015). We therefore asked whether the loss of sister chromatid cohesion in *eso1Δ* cells upon Wpl1 induction was correlated with cohesin release. Wpl1 was induced (TET) or not (DMSO) for 2 h in G2 cells in which the cohesin loader Mis4 was inactivated to prevent further cohesin deposition [cohesin loaded in G2 does not form functional cohesion and is prevented here to focus on stably bound cohesin (Bernard *et al*, 2008; Feytout *et al*, 2011; Vaur *et al*, 2012; Eng *et al*, 2014)]. Cells were released into mitosis and arrested at metaphase (Fig 6A). To ensure that PP4 ablation still suppressed Wpl1-dependent loss of sister chromatid cohesion in this genetic set-up, the status of sister chromatid cohesion was monitored by cen2FISH (Fig 6B). A higher background of sister *cen2* separation was observed in the *mis4-367* background,

consistent with the fact that a fraction of the cell population (typically ~20%) was not yet in G2 at the time of the temperature shift and therefore executed S phase at the restrictive temperature and did not establish sister chromatid cohesion. However, the remaining ~80% had established sister chromatid cohesion at 25°C when the cohesin loader was functional. Accordingly, the FISH analysis showed that PP4 ablation still significantly reduced Wpl1-dependent loss of sister chromatid cohesion in this assay (Fig 6B).

Wpl1-mediated cohesin release was monitored by measuring the amount of DNA-bound cohesin by Rad21-9PK chromatin immunoprecipitation (ChIP) at cohesin-associated regions (CARs) at and around the region covered by the cen2FISH probe (Fig 6C). The ratio ChIP TET/ChIP DMSO (Fig 6D) illustrates the efficiency of Wpl1-dependent cohesin release from DNA (the ratio would be equal to 0 if cohesin was fully dissociated by Wpl1). As expected, Wpl1 induction had little effect in an *eso1*⁺ background. In *eso1Δ*, it was expected that Wpl1 would release cohesin from DNA. However, the reaction was far from complete. The efficiency of Wpl1-dependent cohesin release was variable among CARs, and a

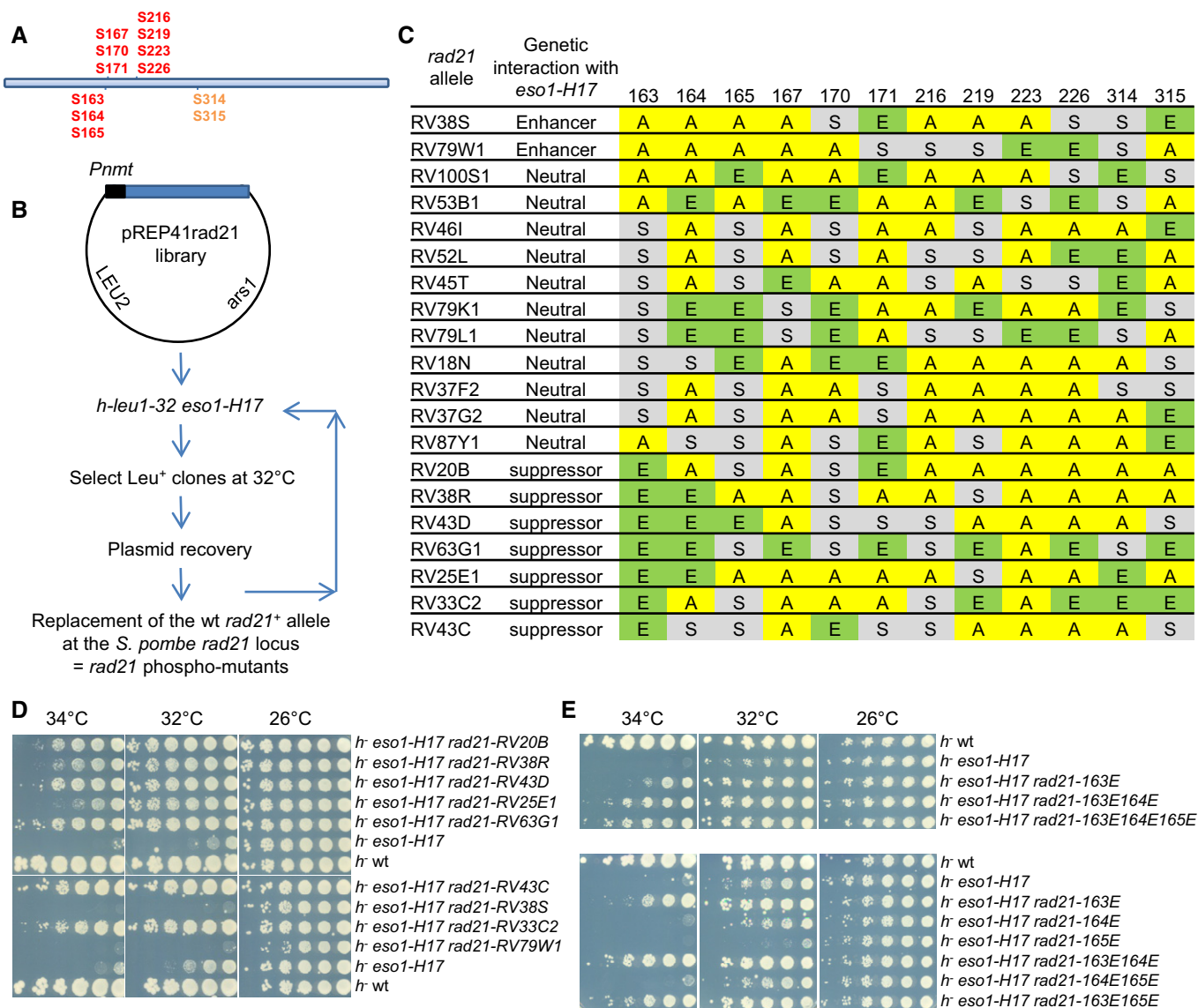


Figure 4. Screen for *rad21* phospho-mutants suppressors of *eso1-H17*.

- A** A combinatorial *rad21* DNA library was synthesized that incorporates either an alanine (non-phosphorylatable), a glutamic acid (phospho-mimicking) or a serine codon for each of the 12 sites shown in the diagram. These include serine residues more frequently phosphorylated in the absence of Pph3 (S164 S165, S216 S219 S226) and their neighbouring serine residues. S314 and S315 were included as they were detected as phosphorylated only in the absence of Pph3 although with low confidence (only in one experiment and two peptides with an ambiguity on the position of the phosphorylated residue, see Dataset EV1).
- B** Workflow of the selection procedure. The *rad21* DNA library was cloned in the pREP41 vector carrying the down-regulated version of the *nmt* promoter and the LEU2 selection marker (Basi *et al*, 1993). The library was transformed into a *leu1-32 eso1-H17* recipient strain. Transformants were allowed to grow for 24 h at 25°C and then shifted to 32°C to select for clones able to grow at the restrictive temperature for *eso1-H17*. Plasmid DNA was recovered from individual clones and transformed again into the *eso1-H17* strain to ensure that suppression was conferred by plasmid DNA. The region surrounding the variable codons was PCR amplified and used to replace the wild-type *rad21*⁺ allele to generate *rad21* phospho-mutants.
- C** Primary amino acid sequence at each of the 12 variable positions encoded by the *rad21* phospho-alleles. Eleven alleles did not modify the restrictive temperature of *eso1-H17*. Two mutants enhanced the thermosensitive phenotype (enhancer) and 7 *rad21* phospho-alleles behaved as *eso1-H17* suppressors. A, alanine; S, serine; E, glutamic acid.
- D** Cell growth assays showing the suppressor/enhancer phenotypes of the selected phospho-mutants.
- E** Cell growth assays showing that a single phospho-mimicking residue at position 163 (S163E) is sufficient to partially suppress the thermosensitive phenotype of *eso1-H17* and the level of suppression is increased with an additional phospho-mimicking residue at position 164 and/or 165.

fraction of Rad21 remained bound to DNA at all sites examined. This indicates that DNA-bound cohesin is made of two sub-populations. Type 1 cohesin behaves as previously described: It is released from DNA in a Wpl1-dependent manner and this is

prevented by Psm3 acetylation [Wpl1 releasing activity was abrogated in a *psm3-K10SK106N* background, mimicking acetylated Psm3 (Fig EV3)]. Type 2 cohesin, however, is not removed from DNA by Wpl1 and remains stably bound although in a non-cohesive state.

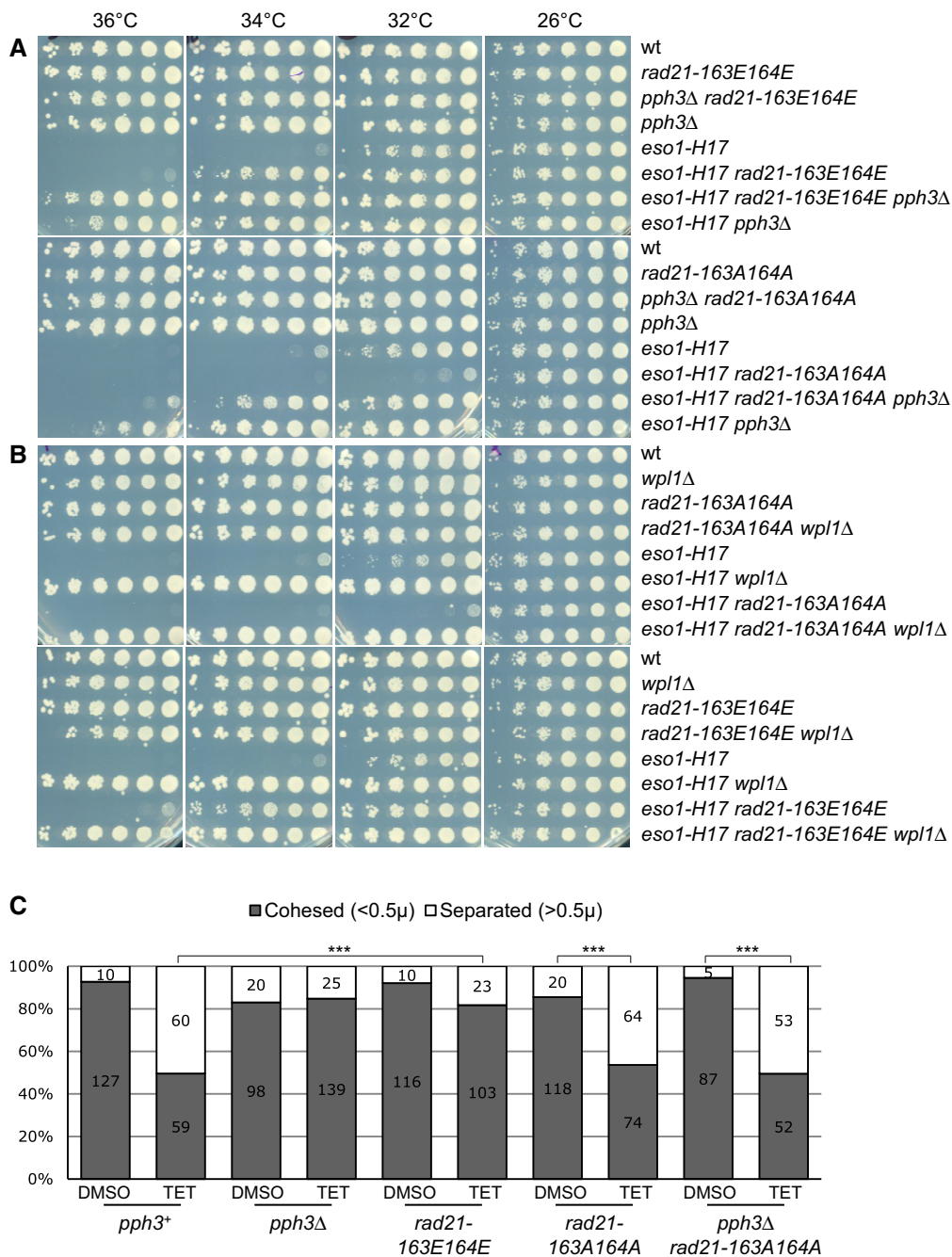


Figure 5. The phosphorylation status of Rad21 S163 S164 regulates Wpl1 anti-cohesion function.

A Cell growth assays showing that *rad21-S163E164E* and *rad21-S163A164A* behave as *eso1-H17* suppressor and enhancer, respectively. Deletion of the *pph3* gene is epistatic on *rad21-163E164E*, and conversely, the suppression by *pph3Δ* is reduced by *rad21-S163A164A*.
 B *wpl1Δ* is epistatic on *rad21* phospho-alleles for *eso1-H17* suppression.
 C Cen2FISH on metaphase cells. Wpl1-MYC was induced in *cdc25-22 wee1-as8 cut9^{ts} eso1Δ* cells as in Fig 2B, and sister chromatid cohesion was monitored by FISH in metaphase-arrested cells using the *cen2* proximal probe. The number of metaphase cells examined is indicated. ****P* < 0.0001 two-sided Fisher's exact test with $\alpha < 0.05$.

Wpl1 requires PP4-mediated Rad21 de-phosphorylation to abolish sister chromatid cohesion mediated by type 2 cohesin

The efficiency of Rad21 release was similar in *eso1Δ psy2Δ* or *eso1Δ pph3Δ* as compared to *eso1Δ* cells (Fig 6D), arguing that

PP4 is dispensable for Wpl1-dependent cohesin removal (type 1 cohesin). However, sister chromatid cohesion was significantly improved when *psy2* was deleted (Fig 6B) implying that the fraction of cohesin that remained DNA-bound (type 2 cohesin) was cohesive in *psy2Δ* but not in *psy2+* cells. These data argue that

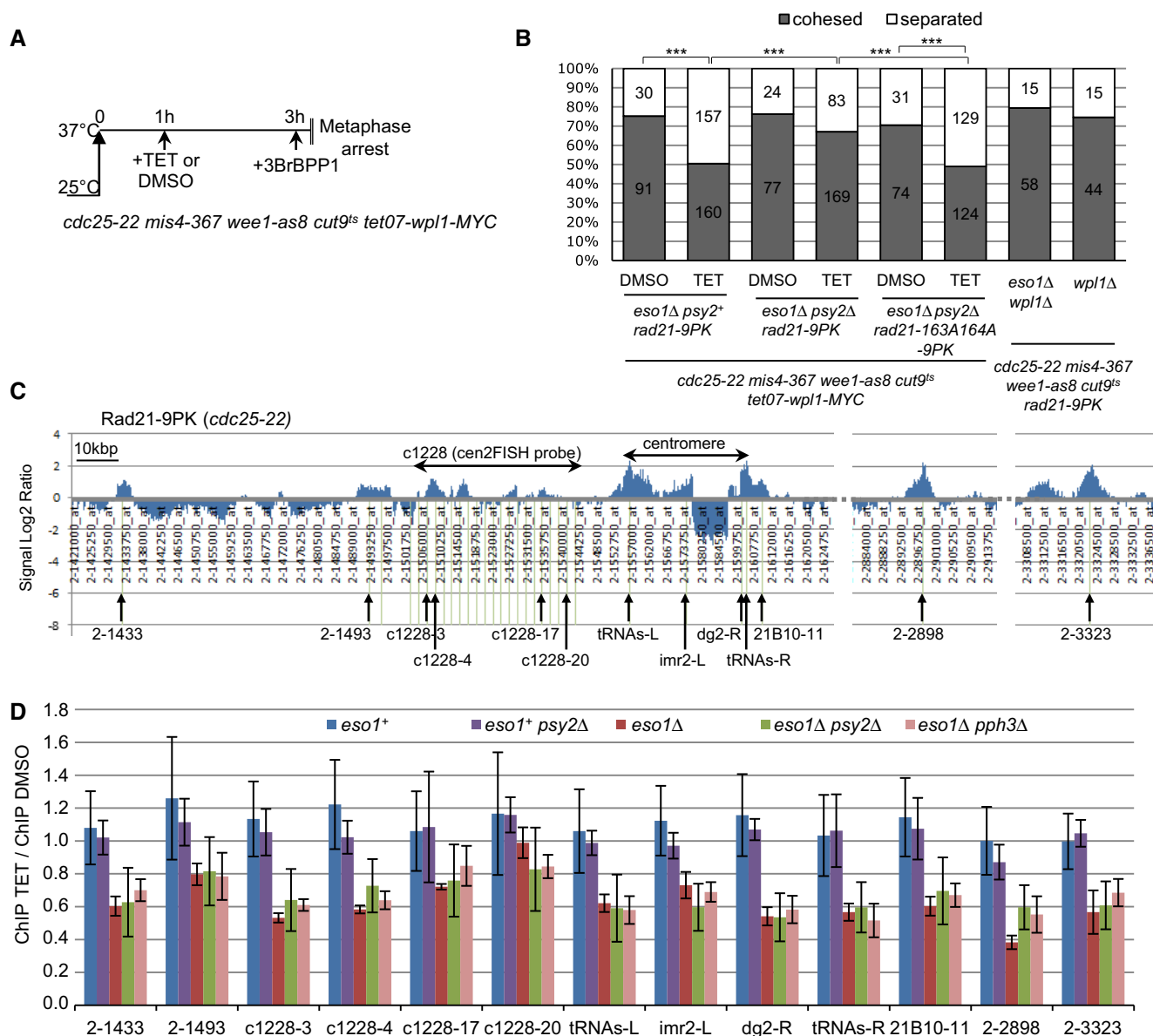


Figure 6. Analysis of chromatin-bound Rad21 after Wpl1 induction.

A Wpl1-MYC was induced as in Fig 2B. The *mis4-367* mutation prevents further cohesin loading at 37°C.

B Cen2FISH on metaphase cells. *** $P < 0.0001$ two-sided Fisher's exact test with $\alpha < 0.05$. The number of metaphase cells examined is indicated.

C Cohesin (Rad21-9PK) map at and around the centromere of chromosome 2 in *cdc25-22* arrested cells (Schmidt et al, 2009) was used to design primer pairs (vertical arrows) for chromatin immunoprecipitation (ChIP).

D Efficiency of Wpl1-dependent Rad21-9PK release from DNA. The ratio ChIP TET/ChIP DMSO was calculated from four ChIPs pairs (mean \pm SD).

Source data are available online for this figure.

type 2 cohesin is not released from chromatin by Wpl1 but becomes non-cohesive through the combined action of Wpl1 and PP4.

The rescue of sister chromatid cohesion by *psy2Δ* was abrogated in a *rad21-163A164A* background (Fig 6B). This confirms that Rad21-S163S164 is a critical PP4 target and reinforces the notion that type 2 cohesion is sensitive to Wpl1 in a manner dependent on Rad21-S163S164 de-phosphorylation by PP4. As expected, the loss of sister chromatid cohesion in a *rad21-163A164A* background was

not correlated with an increase in Wpl1-dependent cohesin release (Fig EV4), consistent with the notion that cohesion is lost by a mechanism distinct from cohesin removal from DNA. It should be noted that *rad21-163A164A* appears to lower the efficiency of Wpl1-mediated cohesin removal at some chromosome arm sites in a *psy2Δ* background. The significance of this is unclear since the effect is weak and often within error bars and additional experiments showed that Wpl1-mediated Rad21 release was very similar in *rad21-163A164A*, *rad21-163E164E* and *psy2Δ*, arguing that PP4

ablation and *rad21* phospho-mutants barely affect Wpl1-dependent Rad21 release from DNA (Fig EV4).

From this analysis, we suggest the existence of two types of cohesin: Type 1 is released from chromatin by Wpl1, while type 2 is not released but becomes non-cohesive through the action of Wpl1-PP4 and one critical PP4 substrate is Rad21.

PP4 de-phosphorylates Rad21 on chromatin and de-phosphorylated Rad21 remains chromatin bound

If this were correct, we would expect Rad21 to become de-phosphorylated while remaining chromatin bound in the above Wpl1 induction experiments. Cell fractionation confirmed that a fraction of Rad21 remained chromatin bound after Wpl1 induction and further showed that chromatin-bound Rad21 remained phosphorylated when Wpl1 was induced in an *eso1*⁺ background, whereas it became de-phosphorylated in a PP4-dependent manner when *eso1* was deleted (Fig 7A). Hence, Wpl1 triggers PP4-dependent Rad21 de-phosphorylation on chromatin without cohesin release. Consistent with the notion that PP4 acts on chromatin, nuclear spreads showed that a fraction of Psy2-FLAG is chromatin bound (Fig EV5). Psy2-FLAG forms foci over a general background of chromatin staining. The foci are mostly distinct from Rad21-9PK foci, indicating that Psy2 is not specifically enriched at cohesin binding sites. A ChIP assay showed that Psy2 is found at Rad21 binding sites although its abundance is not correlated with that of Rad21 (Fig EV5). A fractionation experiment showed that Psy2-FLAG is found both in the soluble and the chromatin fractions. Psy2-FLAG from the soluble pool did not co-immunoprecipitate Wpl1, whereas it did so after solubilization of chromatin proteins by nucleic acid digestion (Fig 7C). This argues that Psy2 contacts Wpl1 on chromatin and additionally shows that the interaction between PP4 and Wpl1 is not dependent on nucleic acid and is likely mediated by protein-protein interactions.

Next we asked whether PP4 recruitment to chromatin and its binding to cohesin were dependent on Wpl1/Pds5. Nuclear spreads showed that Psy2-FLAG bound chromatin independently of Wpl1 and Pds5 and Psy2-FLAG co-immunoprecipitated Psm1 independently of Wpl1, Pds5 and Pph3 (Fig EV5). This piece of data argues that Psy2 does not require Pph3, Wpl1 and Pds5 for cohesin binding although they are all required for PP4-mediated Rad21 de-phosphorylation.

As Rad21 phosphorylation would protect type 2 sister chromatid cohesion from Wpl1 unless erased by PP4, Wpl1 may not bind hyper-phosphorylated Rad21. This seems unlikely since ChIP experiments (Fig EV4) showed that *rad21-163A164A* and *rad21-163E164E* did not affect Wpl1-mediated Rad21 release from DNA, suggesting that the phosphorylation status of these Rad21 residues does not regulate Wpl1 binding to cohesin. Likewise, PP4 ablation did not prevent Rad21 release by Wpl1 (Fig 6). To further strengthen this conclusion, protein extracts were prepared from *pph3Δ* and *psy2Δ* cells in which Rad21 is hyper-phosphorylated. As shown in Fig EV5, Wpl1-MYC still co-immunoprecipitated Rad21, showing that PP4 and Rad21 de-phosphorylation are not required for Wpl1 binding to cohesin.

Altogether, these data indicate that PP4 triggers Rad21 de-phosphorylation on chromatin in a Wpl1-dependent manner and this event triggers the loss of type 2 cohesion without cohesin release

from DNA. PP4 and cohesin appear to interact on chromatin although they may be recruited there independently from each other.

Discussion

From the data presented here, we propose a model involving two types of sister chromatid cohesion (Fig 7D). In type 1 cohesion, sister chromatids would be trapped by cohesin and Wpl1 would disrupt cohesion by opening the Psm3-Rad21 interface resulting in cohesin release from DNA and cohesion loss, as previously proposed (Chan *et al*, 2012; Peters & Nishiyama, 2012; Gligoris *et al*, 2014; Huis in 't Veld *et al*, 2014; Murayama & Uhlmann, 2015; Beckouet *et al*, 2016). This type of cohesion is protected by the Eso1 acetyl-transferase through the acetylation of Psm3. Consistently, Wpl1-dependent cohesin release is prevented when Eso1 is functional or when Eso1 function is bypassed by an acetyl-mimicking form of Psm3. Type 1 cohesion is not regulated by PP4 as PP4 ablation does not prevent cohesin release by Wpl1 when Eso1 is ablated.

In type 2 cohesion, Wpl1 does not provoke cohesin release, but cohesion is nevertheless lost in a Wpl1-dependent manner. Wpl1 triggers Rad21 de-phosphorylation by PP4 without subsequent Rad21 release from chromatin. Here again Eso1 protects sister chromatid cohesion but this time by preventing Wpl1/PP4-mediated de-phosphorylation of Rad21.

A prediction from this model is that sister chromatid cohesion would be retained when only one branch of the pathway is disrupted. Several lines of evidence indicate that the Psm3 acetylation pathway can be disrupted without abrogating sister chromatid cohesion. A non-acetylatable form of Psm3 (Psm3^{K105RK106R}) is viable but lethal when the *eso1* gene is deleted, implying that a second Eso1-dependent pathway is operating to preserve sister chromatid cohesion. Likewise, the *eso1-H17* mutant must preserve this additional function since it is viable although deficient for Psm3^{K106} acetylation at the permissive temperature (Feytout *et al*, 2011).

For type 2 cohesion, PP4 ablation significantly improves sister chromatid cohesion and allows the survival of an *eso1*-deleted strain. Since Psm3 is not acetylated in the absence of Eso1, this implies that sister chromatid cohesion relies on maintaining key PP4 substrates in their phosphorylated state. Rad21 is one of these but is not the sole relevant PP4 substrate as the phospho-mimicking allele *rad21-163E164E* is a weaker *eso1* suppressor than PP4 ablation.

Another prediction from this model is that sister chromatid cohesion would be abrogated when both pathways are disrupted. The non-phosphorylatable allele *rad21-163A164A* did not show any genetic interaction with *psm3*^{K105RK106R}. The reason for this is unclear. The non-acetylatable *psm3* allele may not perfectly mimic the non-acetylated state and/or Eso1 may have other substrates for antagonizing Wpl1. Additionally, *rad21-S163S164* is not the sole relevant PP4 substrate. The rigorous testing of this prediction would require the identification of all relevant PP4 targets and their substitution with non-phosphorylatable alleles.

The kinase(s) responsible for Rad21 phosphorylation are currently unknown. These are unlikely under the control of Eso1

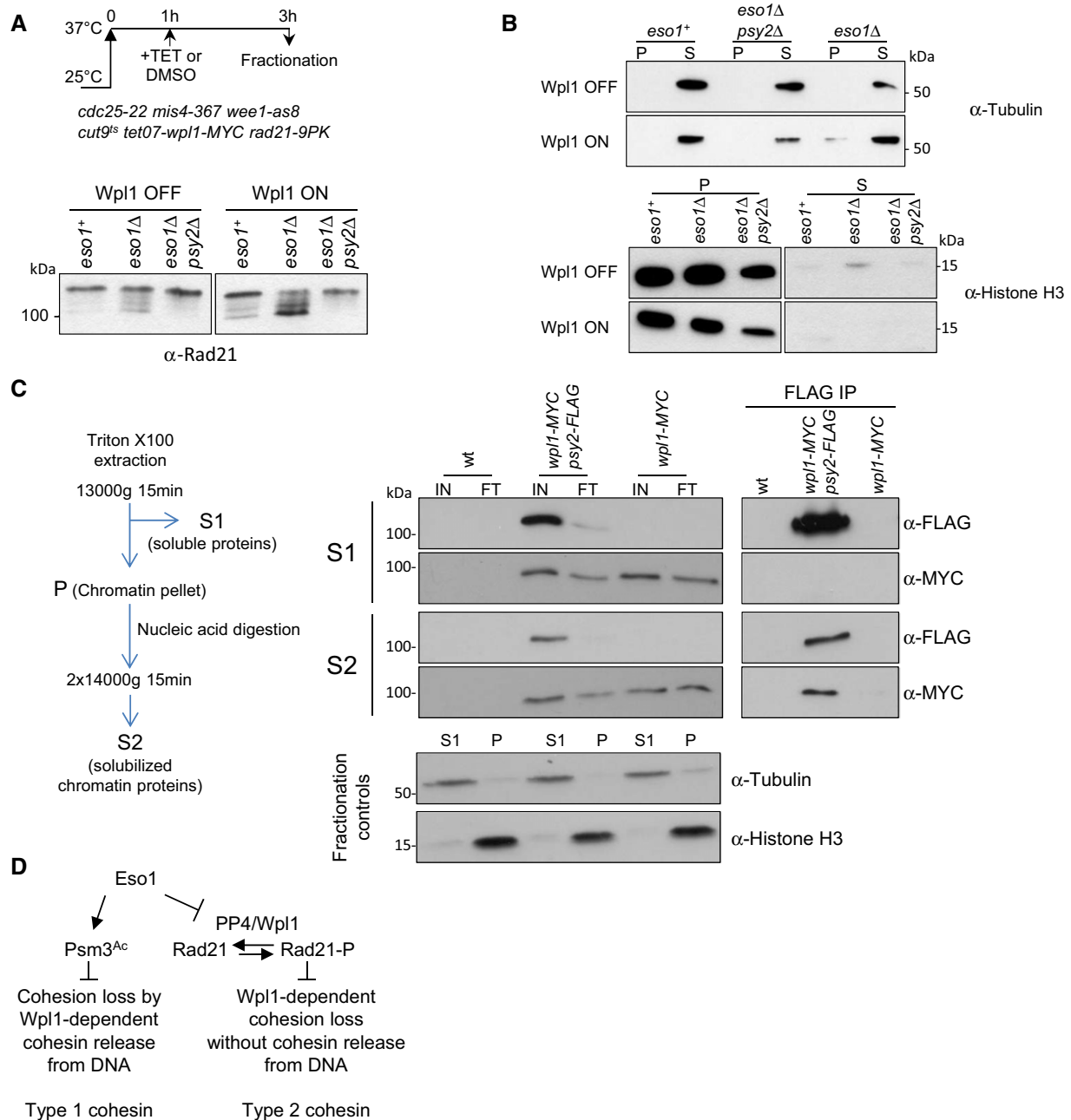


Figure 7. PP4 interacts with Wpl1 and de-phosphorylates Rad21 on chromatin.

- A Rad21 is de-phosphorylated on chromatin in a Wpl1- and PP4-dependent manner in the absence of Eso1. Wpl1 was induced in the indicated strains as in Fig 6. Samples were collected 2 h later, chromatin proteins were extracted and analysed by Western blotting with anti-Rad21 antibodies.
- B Fractionation controls. Tubulin and histone H3 were used as markers for the soluble fraction (S) and the chromatin pellet (P), respectively.
- C PP4 interacts with Wpl1 on chromatin. Exponentially growing cells from the indicated strains were collected. Psy2-FLAG was immunoprecipitated from the soluble fraction (S1) and from chromatin proteins (S2) solubilized by nucleic acid digestion of the chromatin pellet (P). Input, IP and fractionation controls were analysed by Western blotting using the indicated antibodies.
- D Model of Wpl1-PP4 regulation of sister chromatid cohesion.

Source data are available online for this figure.

since chromatin-bound Rad21 remained phosphorylated in an *eso1Δ* background as long as Wpl1 and/or PP4 were not present. However Rad21 remained phosphorylated upon Wpl1 induction when Eso1 was functional, suggesting that Eso1 shelters Rad21 from Wpl1-PP4.

The mechanism does not seem to involve Psm3 acetylation since preventing Psm3 acetylation is not lethal and Rad21 is not hyperphosphorylated in a *psm3* acetyl-mimicking mutant. Another possible mechanism would be that Eso1 prevents PP4 binding to cohesin.

This seems unlikely since Psy2 co-immunoprecipitated cohesin from *eso1*⁺ protein extracts. We cannot rule out that Eso1 may control Pph3 binding to cohesin. This possibility was left unexplored since our attempts to tag Pph3 resulted in non-functional PP4. Alternatively, Eso1 may protect cohesin from PP4 by the acetylation of an unknown substrate or through the recruitment of a sheltering factor.

This study provides evidence for two types of cohesive cohesin and both are negatively regulated by Wpl1. To keep on with current models, we can speculate that type 1 cohesion is abolished by Wpl1 through the release of both sister chromatids from cohesin. By contrast for type 2 cohesion, Wpl1 abolishes cohesion without apparent cohesin release from DNA, suggesting that only one sister chromatid may escape cohesin. This scenario further suggests that the two chromatids may be tethered differently within cohesin. It was shown recently that the two SMC arms can associate with each other in a manner dependent on multiple post-translational modifications within SMC coiled-coils (Kulemzina *et al*, 2016) and coiled-coil interactions have been observed in crosslinking experiments (Huis in 't Veld *et al*, 2014). An intriguing possibility would be that one sister chromatid remain trapped within the SMC's, while the other would be released by Wpl1. Alternatively, type 2 cohesion may stem from cohesin-cohesin interactions regulated by Wpl1 and Rad21 phosphorylation. It is worth mentioning that type 2 cohesin may exist in budding yeast since a pool of cohesin remained stably bound to DNA upon inactivation of Eco1 (Chan *et al*, 2012) and mutations within the kleisin central region impaired sister chromatid cohesion while preserving a stable cohesin-DNA interaction (Eng *et al*, 2014).

We have shown here that the status of Rad21 phosphorylation modulates cohesin susceptibility to Wpl1 with the important implication that sister chromatid cohesion and possibly the other functions of cohesin might be fine-tuned in space and time by altering the balance between kinase and phosphatase activities. The central region of Rad21 is poorly conserved, but numerous phosphorylation sites map to the equivalent region within human Rad21 (<http://www.phosphosite.org/>). Given the conservation of PP4 and cohesin, a similar mechanism may operate across species, including humans.

Materials and Methods

Schizosaccharomyces pombe strains and genetics

General *S. pombe* methods, reagents and media are described in Moreno *et al* (1991). All strains are listed in Table EV1. Experiments were carried out using YES medium unless otherwise stated. Gene deletions and epitope tagging were performed by gene targeting using polymerase chain reaction (PCR) products (Bahler *et al*, 1998). The *tetO7-wpl1-MYC* allele was constructed as follows. A DNA fragment carrying *hphMX-tetO7-Pcyc1* was amplified by PCR using *pFA6a-hphMX-tetO-Pcyc1-3xFLAG* (Zilio *et al*, 2012) as template and oligonucleotides *tetO7-wpl1_fw* (CATTGTGAGTTGGTACGACCGTGTTCTCCATTTTGTAAAGAATCGATGTC AAGCCAGCGGATTGAAGAACCCTTGAAGAATTCGAGCTCGTTTAAAC) and *tetO7-wpl1_rev* (ACGTCTAAAAAGTTCCAAACTTCCGATTCCGAAGAAATTCCTTCAAACCATATCTTTTTCCTTACATTTTCTCTTTTCATATTAATTAACCTCCAGG). The tetracycline sensitive repressor

was introduced by crossing with *ura4*⁺-*tetON* [*tetR-tup11D70* integrated at the *ura4*⁺ locus (Zilio *et al*, 2012)].

Genetic screen for *eso1-H17* suppressors

Cells from strain 4042 (*h*⁺ *eso1-H17 wpl1*⁺-*hygR*) were plated on YES medium, incubated at 25°C until colony formation and then replica plated at 36°C onto YES plates containing the vital dye phloxine B. After 24-h incubation, the replicated colonies stained dark red with phloxine B, insuring that colonies were built from a thermosensitive cell founder. After 2–4 days at 36°C, white growing sectors (suppressors) appeared and were recovered. To screen out mutations within *wpl1* and *eso1-H17*, the suppressors were crossed with 4043 (*h*⁻ *natR-eso1-H17 wpl1Δ::kanR*) and the segregation of the thermosensitive phenotype (Ts) was analysed within the Nat^R Hyg^R progeny. Suppressors arising from *eso1-H17* reversion were expected to yield 100% Ts, whereas those arising from *wpl1* mutation should be 100% non-Ts. Similar crosses with appropriate marked strains were made to identify suppressors linked to the *psm3*, *pvc3* and *pds5* loci. Mutations were identified by PCR amplification of the relevant genes and DNA sequencing. One suppressor called *sup111* segregated against all the above loci and mapped ~20 cM away from the *eso1* locus on chromosome 2. The mutation was identified by comparative genome hybridization (CGH). Genomic DNA was extracted from the suppressor strain and the wild-type *S. pombe* reference strain, SP972 (strain 2 in Table EV1) and co-hybridized to a CGH tiling array (29–32 mer probes with 7 or 8 base spacing from the start of one probe to the start of the next, Roche Nimblegen). The array spanned most of the right arm of chromosome 2, from coordinate 3,220,000 to coordinate 4,720,000 (NC_003423, Genbank version NC_003423.3 GI:162312348). DNA regions carrying candidate single nucleotide polymorphisms (SNPs) were used to design a high-resolution tiling array (29–30 mer probes tiled such as each candidate SNP is analysed by eight probes, four on each DNA strand). A single G to A SNP (R111W) was found at position 395,548 within SPBC26H8.05c (*pph3*). The mutation was confirmed by PCR and DNA sequencing from two independent *sup111* and wt strains. The *pph3* gene was deleted and genetic analyses showed that *pph3Δ* was allelic to *sup111* and suppressed the Ts phenotype of *eso1-H17*.

Screening of a *rad21* phospho-mutant library and creation of *rad21* phospho-mutants

The library of *rad21* phospho-alleles was synthesized and cloned by ThermoFisher Scientific. The entire *rad21* open reading frame was synthesized with randomized codons Ser (33.3%), Ala (33.3%), Glu (33.3%) at each of the 12 chosen positions (163, 164, 165, 167, 170, 171, 216, 219, 223, 226, 314, 315) and the library cloned as NdeI/XmaI fragments into pREP41 (Basi *et al*, 1993).

The library was transformed into strain 2960 (*eso1-H17 leu1-32*) and cells plated on PMG to select for Leu⁺ transformants. After 24 h at 25°C, plates were transferred to 32°C (a restrictive temperature for *eso1-H17* on minimal medium) to select for clones able to rescue the thermosensitive phenotype of *eso1-H17*. Plasmid DNA was recovered by transformation of *Escherichia coli* and transformed back into strain 2960 to verify that plasmid DNA suppressed the Ts phenotype of *eso1-H17*.

The *rad21* mutant alleles were created by two-step gene replacement. As *rad21* is essential for cell survival, the constructions were made in a *psm3-rad21* gene fusion background which renders the endogenous *rad21* gene dispensable (Chan *et al*, 2012). A portion of the *rad21* ORF (from nucleotide 486 to 945) was replaced with the *ura4⁺* gene by one-step gene replacement using a PCR fragment generated with primers *rad21d(486–945)ura4-fw* CATTGATTTTC AATGGTCTCAACTTCTTCGTACACCCTCTCGTTCTTCGAACACTCT TGAACACTACATTCTTTACCAATATAGCTACAAATCCCAGCTGGC and *rad21d(486–945)ura4-rev* TCAACAACCTGACCTTCTCTACTCCTG CTGCTGCAGGACGAGATGAATCATCTTCCATAATGTCAGAAGGGA GATGAATTGTGGTAATGTTGTAGGAGC and the *ura4⁺* gene as a template. The *ura4⁺* sequence was then replaced by homologous recombination with a 1,325-bp DNA fragment amplified from the pREPrad21 plasmids carrying the *rad21* alleles of interest using primers *rad21+45_FW* (AAGGTATGGTTGGCAGCTCAC) and *rad21+1,369_rev* (TCAGTACGTTGGTGGCTTGGC). *Ura⁻* clones were selected on 5-fluoroorotic acid containing plates. Correct gene replacement was confirmed by PCR and DNA sequencing of the entire *rad21* gene and the strains backcrossed to eliminate the *psm3-rad21* gene fusion and auxotrophic markers. Twenty *rad21* mutants were generated and placed into an *eso1-H17* background to select for those able to suppress the thermosensitive phenotype.

Wpl1-MYC induction experiments

All strains carried the thermosensitive *cdc25-22* mutation that prevents entry into mitosis at 37°C. Cells were grown to early log phase at 25°C and shifted to 37°C. In a typical experiment, Wpl1-MYC was induced after 1 h at 37°C by the addition of 5 µg/ml tetracycline (anhydrotetracycline hydrochloride, SIGMA, stock solution 10 mg/ml in DMSO) or DMSO alone for the un-induced condition and the cells kept at 37°C for an additional 2 h. To assess chromosome segregation during the following mitosis, the cultures were shifted back to 25°C. Cells entered mitosis synchronously and were fixed with 70% ethanol 80 min after transfer to 25°C at which time anaphase cells were the most abundant. Fixed cells were rehydrated in PBS, stained with DAPI and observed by fluorescence microscopy. Aberrant mitoses were defined by the presence of DAPI-stained material lagging along the cell axis. For FISH and ChIP experiments, cells were released from the *cdc25-22* arrest by the inhibition of Wee1-as8 with 30 µM 3BrBPP1 (Toronto Research Chemicals Inc., stock solution 50 mM in methanol) and arrested at metaphase by the thermosensitive *cut9^{ts}* mutation as described (Tay *et al*, 2013). Cells were collected 30 min after 3BrBPP1 addition, at which time the cell population was mainly composed of metaphase cells (~90% cells with condensed chromosomes and loss of the interphase array of microtubules and 70–80% with a metaphase spindle, as seen by DAPI and tubulin staining).

Fluorescence *in situ* hybridization (FISH)

Cells were fixed by the addition of paraformaldehyde to a final concentration of 1.8% in 1.2 M sorbitol. The flasks were removed from 37°C, incubated at 21°C for 45 min and processed for tubulin staining using TAT1 antibodies (Woods *et al*, 1989). Cells were re-fixed and processed for FISH as described (Steglich *et al*, 2015) using the centromere linked c1228 cosmid as a probe (Mizukami

et al, 1993). Metaphase cells were imaged using a Leica DMRXA microscope and a 100× objective. Distances between FISH signals were measured from maximum projections of images created from z-series of eight 0.4-µm steps using MetaMorph software. Cen2FISH signals were considered as separated when the distance was > 0.5 µm. This cut-off was chosen as most (~95%) wild-type metaphase-arrested cells had cen2FISH signals separated by a distance < 0.5 µm (Feytout *et al*, 2011). Statistical analysis was done with the GraphPad Prism software using two-tailed Fisher's exact test with 95% confidence interval. The number of metaphase cells analysed is indicated within the graphs.

Chromatin immunoprecipitation

The procedure was as described (Feytout *et al*, 2011) with the following modifications. Cells were fixed for 15 min at 37°C with 2.54% formaldehyde (SIGMA). Fixation was stopped by the addition of 0.125 M glycine and transfer on ice for 5 min. DNA was recovered using ChIP DNA Clean & Concentrator columns (Zymo Research). ChIP enrichments were calculated as % DNA immunoprecipitated at the locus of interest relative to the input sample. For Rad21-9PK ChIP, the data presented (Figs 6 and EV4) are the ratio ChIP TET/ChIP DMSO calculated from four technical replicates (4 ChIP TET and 4 ChIP DMSO) with error bars representing standard deviation. Key experiments (in an *eso1⁺*, *eso1Δ*, *eso1Δ pys2Δ* and *eso1Δ pys2Δ rad21-163A164A* background) were reproduced independently at least twice. FLAG ChIP (Fig EV5) was done using mouse monoclonal anti-FLAG M2 (F1804, SIGMA) using 2 µg per ChIP. A single ChIP was made and the enrichment calculated from duplicate qPCRs.

Nuclear spreads

Nuclear spreads were done as described (Bernard *et al*, 2008) with the following modifications. Immuno-detection was performed with monoclonal anti-FLAG M2 (F1804, 2 µg/ml) for Psy2-FLAG and rabbit polyclonal anti-V5 (Abcam, 2 µg/ml) in PBS buffer containing 1% BSA. Secondary antibodies were anti-rabbit IgG-FITC (SIGMA F0382, 1:400) and anti-mouse IgG-CY3 (Jackson 115-165-003, 1:1,000) in PBS 1% BSA. The images presented were captured with a 100× objective. Fluorescence quantification was done from images collected with a 63× objective, and the data presented are the mean ± 95% confidence interval of the mean with $\alpha = 0.05$, as described previously (Bernard *et al*, 2008).

General protein methods

Protein extracts, IPs and Western blotting were done as described (Feytout *et al*, 2011). Rabbit polyclonal antibodies against Psm1 and Psm3 have been described previously (Dheur *et al*, 2011; Feytout *et al*, 2011). Rad21 polyclonal antibodies were raised in rabbits against the C-terminus last 413 amino acids of the protein as previously described (Birkenbihl & Subramani, 1995) and immunopurified with the same peptide. Anti-PK (monoclonal mouse anti-V5) is from AbD Serotec, anti-FLAG (mouse monoclonal anti-FLAG M2, F1804) from SIGMA, mouse monoclonal anti-MYC (9E10) from Santa Cruz, anti-tubulin (mouse monoclonal) from (Woods *et al*, 1989), rabbit polyclonal to histone H3 (ab1791) from Abcam.

Lambda phosphatase treatment of Rad21 was performed on Rad21-9PK immunoprecipitated from total cell extracts. Rad21-9PK bound to magnetic beads was washed twice in phosphatase buffer (50 mM HEPES; 100 mM NaCl; 2 mM DTT; 0.01% Brij 35 pH 7.5) and beads dispensed into three 50- μ l aliquots (without phosphatase, 400 units phosphatase (New England Biolabs), 400 units phosphatase and 50 mM Na-vanadate and 10 mM β -glycerophosphate). $MnCl_2$ was added to 1 mM and reactions were carried out for 40 min at 30°C, stopped by addition of Laemmli buffer and heating for 10 min at 95°C.

Cell fractionation

Cell fractionation was performed as described using 1% Triton X-100 buffer for extraction of non-chromatin proteins (Schmidt *et al*, 2009). Co-IP experiments after fractionation were done as follows. The soluble fraction was recovered, clarified twice by centrifugation (13,000 g 10 min 4°C) and subjected to IP with anti-FLAG antibodies. The chromatin pellet was dissolved in extraction buffer, and nucleic acids were digested by the addition of Benzonase (100 U) and 1-h incubation on ice. Insoluble material was removed by two successive rounds of centrifugation (14,000 g 10 min 4°C) and the supernatant subjected to IP with anti-FLAG antibodies.

Mass spectrometry

Rad21 analysis was conducted from five individual mass spectrometry experiments. Rad21-9PK was immunopurified from strains 3789 (wt) and 6284 (*pph3 Δ*) using 10^{10} cells grown to late log phase at 25°C. Rad21-9PK was eluted in 50 μ l of Laemmli buffer and the sample loaded onto a preparative 8% PAGE. After a short electrophoresis, the gel was stained with Colloidal Blue and the protein containing band was excised. Gel pieces were destained in 25 mM ammonium bicarbonate 50% ACN, rinsed twice in ultrapure water and shrunk in ACN for 10 min. The proteases used were trypsin (Proteomic Grade from SIGMA), GluC, chymotrypsin, thermolysine or elastase (Sequencing Grade from Promega).

After ACN removal, gel pieces were dried at room temperature, covered with the enzyme solution (10 ng/ μ l in 40 mM NH_4HCO_3 and 10% ACN for trypsin; 10 ng/ μ l in 25 mM NH_4HCO_3 and 4% CAN pH 4 for GluC), rehydrated at 4°C for 10 min and finally incubated overnight at 37°C for trypsin or 25°C for GluC. When GluC and trypsin were used in combination, GluC digestion was performed prior to trypsinolysis. Chymotrypsin digestion was conducted overnight at 25°C in Tris-HCl 100 mM, 10 mM $CaCl_2$ pH 8. Thermolysine digestion was conducted overnight at 70°C in 50 mM Tris-HCl 0.5 mM $CaCl_2$ pH 7.8 and elastase digestion overnight at 37°C in Tris-HCl 50 mM pH9.

After proteolysis, supernatants were collected, and an $H_2O/ACN/HCOOH$ (47.5:47.5:5) extraction solution was added onto gel pieces for 15 min. The extraction step was repeated twice. Supernatants were pooled and concentrated down to 40 μ l before addition of formic acid (0.1% final concentration). Samples were stored at -20°C.

The peptide mixtures were analysed on an Ultimate 3000 nanoLC system (Dionex) coupled to a nanospray LTQ-Orbitrap XL mass

spectrometer (ThermoFinnigan, San Jose, CA, USA) or an Electro-spray Q-Exactive quadrupole Orbitrap benchtop mass spectrometer (Thermo Fisher Scientific, San Jose, CA, USA).

nLC-MS/MS analysis with LTQ-Orbitrap XL was done as follows. Ten microlitres of peptide digests was loaded onto a 300 μ m inner diameter \times 5-mm C18 PepMapTM trap column (LC Packings) at a flow rate of 30 μ l/min. The peptides were eluted from the trap column onto an analytical 75-mm id \times 15-cm C18 Pep-Map column (LC Packings) with a 5–40% linear gradient of solvent B in 95 min (solvent A was 0.1% formic acid in 5% ACN, and solvent B was 0.1% formic acid in 80% ACN). The separation flow rate was set at 200 nl/min. The mass spectrometer operated in positive ion mode at a 1.8-kV needle voltage and a 41-V capillary voltage. Data were acquired in a data-dependent mode, alternating an FTMS scan survey over the range m/z 300–1,700 and six ion trap MS/MS scans with CID (collision-induced dissociation) as activation mode. MS/MS spectra were acquired using a 3- m/z unit ion isolation window and normalized collision energy of 35. Mono-charged ions and unassigned charge-state ions were rejected from fragmentation. Dynamic exclusion duration was set to 30 s.

nLC-MS/MS analysis QX was done by loading ten microlitres of peptide digests onto a 300- μ m inner diameter \times 5-mm C18 PepMapTM trap column (LC Packings) at a flow rate of 30 μ l/min. The peptides were eluted from the trap column onto an analytical 75-mm id \times 15-cm C18 Pep-Map column (LC Packings) with a 4–40% linear gradient of solvent B in 108 min (solvent A was 0.1% formic acid in 5% ACN, and solvent B was 0.1% formic acid in 80% ACN). The separation flow rate was set at 300 nl/min. The mass spectrometer operated in positive ion mode at a 1.8-kV needle voltage. Data were acquired using Xcalibur 2.2 software in a data-dependent mode. MS scans (m/z 300–2,000) were recorded at a resolution of $R = 70,000$ (@ m/z 200) and an AGC target of 1×10^6 ions collected within 100 ms. Dynamic exclusion was set to 30 s, and top 15 ions were selected from fragmentation in HCD mode. MS/MS scans with a target value of 1×10^5 ions were collected with a maximum fill time of 120 ms and a resolution of $R = 35,000$. Additionally, only +2 and +3 charged ions were selected for fragmentation. Other settings were as follows: no sheath nor auxiliary gas flow, heated capillary temperature, 200°C; normalized HCD collision energy of 25% and an isolation width of 3 m/z .

Data were searched by SEQUEST through Proteome Discoverer 1.4 (ThermoFisher Scientific Inc.) against the Rad21-9PK sequence embedded in the *S. pombe* Reference Proteome Set (Uniprot version 2014-06; 5,092 entries). Spectra from peptides higher than 5,000 Da or lower than 350 Da were rejected. The search parameters were as follows: Precursor tolerance was set to 10 ppm and fragment tolerance was set at 0.02 Da for FTMS MS/MS data or 0.6 Da for In Trap MS/MS data. Only b- and y-ions were considered for mass calculation. Oxidation of methionine (+16 Da) and phosphorylation (+80 Da) was considered as variable modifications, and carbamidomethylation of cysteines (+57 Da) was considered as fixed modification. Two missed trypsin cleavages were allowed. Peptide validation was performed using Percolator algorithm (Kall *et al*, 2007), and only “high confidence” peptides were retained corresponding to a 1% false-positive rate at peptide level.

Phosphorylation site localization and quantitative analysis

To ascertain phosphorylation sites, localization PhosphoRS 3.1 (Taus *et al*, 2011) implemented in Proteome Discoverer was used and a cut-off of 95% for the site probability was applied. MS/MS spectra were visually inspected.

Label-free quantification of peptides was performed using Progenesis Q1 for Proteomics (v2.0). LC-MS raw data from independent protein bands were imported and aligned automatically to correct for both *m/z* and retention time possible shifts. Alignment quality was manually inspected. Peptide ion features detection was performed in the automatic mode with the highest sensitivity. Peptide intensity versus retention time profiles were generated from which area under the curve (AUC) were calculated. Import of LC/MS database search reports allowed building a matrix indicating abundancies for all detected peptides across all compared samples/bands.

Finally, AUC ratios were calculated and normalized based on the ratio median of unmodified peptides. All conducted experiments are listed in Dataset EV1 (Sheet “Experiments”). Database search results are grouped according to strain (3789 versus 6284) and instruments (LTQ-Orbitrap versus QExactive), see sheets “3789-QX”, “6284-QX”, “3789-Orbi” and “6284-Orbi”.

Expanded View for this article is available online.

Acknowledgements

We thank our colleagues Iain Hagan and Nicolas Zilio for the kind gift of reagents and strains, Damien Laporte and Isabelle Sagot for help with microscopy and Marta Tormos-Perez for critical reading of the manuscript. This work was supported by the Centre National de la Recherche Scientifique, l'Université de Bordeaux, la Région Aquitaine, l'Association pour la Recherche sur le Cancer (PJA 2013 1200 205) and l'Agence Nationale de la Recherche (ANR-14-CE10-0020-01). Adrien Birot was supported by a fellowship from the Agence Nationale de la Recherche Investissements d'Avenir ANR-10-IDEX-03-02 and by l'Association pour la Recherche sur le Cancer (DOC20160603884). Karen Eguienta was supported by a fellowship from the Ministère de l'Enseignement Supérieur et de la Recherche. Karl Ekwall was supported by grants from the Swedish Research Council and Cancer Society.

Author contributions

SVau and JPJ contributed to the conception and design of the study. AB, KEg, SVau and JPJ performed experiments with the technical assistance of SVaz. SC and MB performed mass spectrometry analyses. SVau, AB and JPJ contributed to data analysis and interpretation. JPJ drafted the manuscript with inputs from SVau, AB and KEg. All authors contributed to editing of the manuscript. JPJ and KEg obtained funding and JPJ supervised the study.

Conflict of interest

The authors declare that they have no conflict of interest.

References

Adachi Y, Kokubu A, Ebe M, Nagao K, Yanagida M (2008) Cut1/separase-dependent roles of multiple phosphorylation of fission yeast cohesion subunit Rad21 in post-replicative damage repair and mitosis. *Cell Cycle* 7: 765–776

- Bahler J, Wu JQ, Longtine MS, Shah NG, McKenzie A III, Steever AB, Wach A, Philippsen P, Pringle JR (1998) Heterologous modules for efficient and versatile PCR-based gene targeting in *Schizosaccharomyces pombe*. *Yeast* 14: 943–951
- Basi G, Schmid E, Maundrell K (1993) TATA box mutations in the *Schizosaccharomyces pombe nmt1* promoter affect transcription efficiency but not the transcription start point or thiamine repressibility. *Gene* 123: 131–136
- Beckouet F, Srinivasan M, Roig MB, Chan KL, Scheinost JC, Batty P, Hu B, Petela N, Gligoris T, Smith AC, Strmecki L, Rowland BD, Nasmyth K (2016) Releasing activity disengages cohesin's Smc3/Sccl interface in a process blocked by acetylation. *Mol Cell* 61: 563–574
- Bernard P, Schmidt CK, Vaur S, Dheur S, Drogat J, Genier S, Ekwall K, Uhlmann F, Javerzat JP (2008) Cell-cycle regulation of cohesin stability along fission yeast chromosomes. *EMBO J* 27: 111–121
- Birkenbihl RP, Subramani S (1995) The rad21 gene product of *Schizosaccharomyces pombe* is a nuclear, cell cycle-regulated phosphoprotein. *J Biol Chem* 270: 7703–7711
- Carlson CR, Grallert B, Stokke T, Boye E (1999) Regulation of the start of DNA replication in *Schizosaccharomyces pombe*. *J Cell Sci* 112(Pt 6): 939–946
- Chan KL, Roig MB, Hu B, Beckouet F, Metson J, Nasmyth K (2012) Cohesin's DNA exit gate is distinct from its entrance gate and is regulated by acetylation. *Cell* 150: 961–974
- Cohen PT, Philp A, Vazquez-Martin C (2005) Protein phosphatase 4—from obscurity to vital functions. *FEBS Lett* 579: 3278–3286
- Dheur S, Saupé SJ, Genier S, Vazquez S, Javerzat JP (2011) Role for cohesin in the formation of a heterochromatic domain at fission yeast subtelomeres. *Mol Cell Biol* 31: 1088–1097
- Elbatsh AM, Haarhuis JH, Petela N, Chapard C, Fish A, Celie PH, Stadnik M, Ristic D, Wyman C, Medema RH, Nasmyth K, Rowland BD (2016) Cohesin releases DNA through asymmetric ATPase-driven ring opening. *Mol Cell* 61: 575–588
- Eng T, Guacci V, Koshland D (2014) ROCC, a conserved region in cohesin's Mcd1 subunit, is essential for the proper regulation of the maintenance of cohesion and establishment of condensation. *Mol Biol Cell* 25: 2351–2364
- Eng T, Guacci V, Koshland D (2015) Interallelic complementation provides functional evidence for cohesin-cohesin interactions on DNA. *Mol Biol Cell* 26: 4224–4235
- Feytout A, Vaur S, Genier S, Vazquez S, Javerzat JP (2011) Psm3 acetylation on conserved lysine residues is dispensable for viability in fission yeast but contributes to Eso1-mediated sister chromatid cohesion by antagonizing Wpl1. *Mol Cell Biol* 31: 1771–1786
- Gandhi R, Gillespie PJ, Hirano T (2006) Human Wapl is a cohesin-binding protein that promotes sister-chromatid resolution in mitotic prophase. *Curr Biol* 16: 2406–2417
- Gerlich D, Koch B, Dupeux F, Peters JM, Ellenberg J (2006) Live-cell imaging reveals a stable cohesin-chromatin interaction after but not before DNA replication. *Curr Biol* 16: 1571–1578
- Gligoris TG, Scheinost JC, Burmann F, Petela N, Chan KL, Uluocak P, Beckouet F, Gruber S, Nasmyth K, Lowe J (2014) Closing the cohesin ring: structure and function of its Smc3-kleisin interface. *Science* 346: 963–967
- Haering CH, Farcas AM, Arumugam P, Metson J, Nasmyth K (2008) The cohesin ring concatenates sister DNA molecules. *Nature* 454: 297–301
- Huang CE, Milutinovich M, Koshland D (2005) Rings, bracelet or snaps: fashionable alternatives for Smc complexes. *Philos Trans R Soc Lond B Biol Sci* 360: 537–542

- Huis in 't Veld PJ, Herzog F, Ladurner R, Davidson IF, Piric S, Kreidl E, Bhaskara V, Aebersold R, Peters JM (2014) Characterization of a DNA exit gate in the human cohesin ring. *Science* 346: 968–972
- Kagami A, Sakuno T, Yamagishi Y, Ishiguro T, Tsukahara T, Shirahige K, Tanaka K, Watanabe Y (2011) Acetylation regulates monopolar attachment at multiple levels during meiosis I in fission yeast. *EMBO Rep* 12: 1189–1195
- Kall L, Canterbury JD, Weston J, Noble WS, MacCoss MJ (2007) Semi-supervised learning for peptide identification from shotgun proteomics datasets. *Nat Methods* 4: 923–925
- Kueng S, Hegemann B, Peters BH, Lipp JJ, Schleiffer A, Mechtler K, Peters JM (2006) Wapl controls the dynamic association of cohesin with chromatin. *Cell* 127: 955–967
- Kulemzina I, Ang K, Zhao X, Teh JT, Verma V, Suranthran S, Chavda AP, Huber RG, Eisenhaber B, Eisenhaber F, Yan J, Ivanov D (2016) A reversible association between Smc coiled coils is regulated by lysine acetylation and is required for cohesin association with the DNA. *Mol Cell* 63: 1044–1054
- Mizukami T, Chang WI, Garkavtsev I, Kaplan N, Lombardi D, Matsumoto T, Niwa O, Kounosu A, Yanagida M, Marr TG, Beach D (1993) A 13 kb resolution cosmid map of the 14 Mb fission yeast genome by nonrandom sequence-tagged site mapping. *Cell* 73: 121–132
- Moreno S, Klar A, Nurse P (1991) Molecular genetic analysis of fission yeast *Schizosaccharomyces pombe*. *Methods Enzymol* 194: 795–823
- Murayama Y, Uhlmann F (2015) DNA entry into and exit out of the cohesin ring by an interlocking gate mechanism. *Cell* 163: 1628–1640
- Nasmyth K, Haering CH (2009) Cohesin: its roles and mechanisms. *Annu Rev Genet* 43: 525–558
- Nishiyama T, Ladurner R, Schmitz J, Kreidl E, Schleiffer A, Bhaskara V, Bando M, Shirahige K, Hyman AA, Mechtler K, Peters JM (2010) Sororin mediates sister chromatid cohesion by antagonizing Wapl. *Cell* 143: 737–749
- Peters JM, Nishiyama T (2012) Sister chromatid cohesion. *Cold Spring Harb Perspect Biol* 4: a011130
- Remeseiro S, Losada A (2013) Cohesin, a chromatin engagement ring. *Curr Opin Cell Biol* 25: 63–71
- Schmidt CK, Brookes N, Uhlmann F (2009) Conserved features of cohesin binding along fission yeast chromosomes. *Genome Biol* 10: R52
- Steglich B, Stralfors A, Khorosjutina O, Persson J, Smialowska A, Javerzat JP, Ekwall K (2015) The Fun30 chromatin remodeler Fft3 controls nuclear organization and chromatin structure of insulators and subtelomeres in fission yeast. *PLoS Genet* 11: e1005101
- Surcel A, Koshland D, Ma H, Simpson RT (2008) Cohesin interaction with centromeric minichromosomes shows a multi-complex rod-shaped structure. *PLoS One* 3: e2453
- Tanaka K, Yonekawa T, Kawasaki Y, Kai M, Furuya K, Iwasaki M, Murakami H, Yanagida M, Okayama H (2000) Fission yeast Eso1p is required for establishing sister chromatid cohesion during S phase. *Mol Cell Biol* 20: 3459–3469
- Taus T, Kocher T, Pichler P, Paschke C, Schmidt A, Henrich C, Mechtler K (2011) Universal and confident phosphorylation site localization using phosphoRS. *J Proteome Res* 10: 5354–5362
- Tay YD, Patel A, Kaemena DF, Hagan IM (2013) Mutation of a conserved residue enhances the sensitivity of analogue-sensitized kinases to generate a novel approach to the study of mitosis in fission yeast. *J Cell Sci* 126: 5052–5061
- Vaur S, Feytout A, Vazquez S, Javerzat JP (2012) Pds5 promotes cohesin acetylation and stable cohesin-chromosome interaction. *EMBO Rep* 13: 645–652
- Watrin E, Kaiser FJ, Wendt KS (2016) Gene regulation and chromatin organization: relevance of cohesin mutations to human disease. *Curr Opin Genet Dev* 37: 59–66
- Woods A, Sherwin T, Sasse R, MacRae TH, Baines AJ, Gull K (1989) Definition of individual components within the cytoskeleton of *Trypanosoma brucei* by a library of monoclonal antibodies. *J Cell Sci* 93: 491–500
- Zhang N, Kuznetsov SG, Sharan SK, Li K, Rao PH, Pati D (2008) A handcuff model for the cohesin complex. *J Cell Biol* 183: 1019–1031
- Zilio N, Wehrkamp-Richter S, Boddy MN (2012) A new versatile system for rapid control of gene expression in the fission yeast *Schizosaccharomyces pombe*. *Yeast* 29: 425–434